PROCEEDINGS OF THE ROYAL SOCIETY A

rspa.royalsocietypublishing.org

Research

Article submitted to journal

Subject Areas:
applied mathematics

Keywords:
gravity-capillary, solitary wave, periodic wave, breather

Author for correspondence:
Paul A. Milewski
e-mail: p.a.milewski@bath.ac.uk

Transversally-Periodic Solitary Gravity-Capillary Waves

Paul A. Milewski[1] and Zhan Wang[2]

[1]Department of Mathematical Sciences, University of Bath, Bath, BA2 7AY, UK.
[2]Department of Mathematics, University College London, Gower Street, London, WC1E 6BT, UK.

When both gravity and surface tension effects are present, surface solitary water waves are known to exist in both two- and three-dimensional infinitely deep fluids. We describe here solutions bridging these two cases: travelling waves which are localised in the propagation direction and periodic in the transverse direction. These transversally-periodic gravity-capillary solitary waves are found to be of either elevation or depression type, tend to plane waves below a critical transverse period and tend to solitary lumps as the transverse period tends to infinity. The waves are found numerically in a Hamiltonian system for water waves simplified by a cubic truncation of the Dirichlet to Neumann operator. This approximation has been proven to be very accurate for both two- and three-dimensional computations of fully localised gravity-capillary solitary waves [23]. The stability properties of these waves are then investigated via the time evolution of perturbed wave profiles.

1. Introduction

Gravity-capillary waves are of interest because they affect energy, momentum [13] and material fluxes through the sea surface [6], and because the initial generation of waves by wind is predominantly in the gravity-capillary regime ($\lambda \sim 1$cm) [25]. The study of nonlinear waves and their dynamics in this regime can therefore lead to increased understanding of these phenomena. In this paper we consider the problem of travelling nonlinear gravity-capillary waves localised in the propagation direction and periodic in the transverse direction on an ideal fluid of infinite depth. The latter approximation is physically appropriate even in water only a few centimetres deep, given the waves' small horizontal length scales compared to depth.

Royal Society Publishing
Informing the science of the future

There has been extensive work on solitary gravity-capillary waves in both two- and three-dimensional flows. For a two-dimensional fluid domain (corresponding to a one-dimensional free surface and henceforth denoted as the "1D problem"), the first numerical study of gravity-capillary (GC) solitary waves in deep water was by Longuet-Higgins [12] who computed the wave profiles of a branch of GC solitary waves (so-called depression waves) from the full Euler equations. These solitary waves bifurcate from linear waves at the *finite* wavenumber where the phase speed is a minimum, or, equivalently, when phase and group speeds are equal. Since they bifurcate at finite wavenumber, the solitary waves have oscillatory tails and appear as *steadily* travelling wave packets at small amplitude. More extensive numerical computations were carried out [22] [8] completing the bifurcation diagram, and finding another branch: that of elevation solitary waves. The longitudinal stability of these two branches was studied using a numerical eigenvalue analysis by linearizing about these states in [4] showing that, for small amplitude, depression waves are stable and elevation waves are unstable. The evolution of these instabilities, together with computations of solitary wave collisions, were confirmed in direct numerical simulations of the full equations in [16].

For a three-dimensional fluid domain, *fully localised* 2D steadily travelling waves, often called *lumps*, were first computed in the fluid equations by Părău et. al. [18], with related work in [10], [14] and [2] on reduced models. These localised states are predicted to be unstable at small amplitude based on the behaviour of the two-dimensional focussing nonlinear Schrödinger equation which approximates these solutions (see below). More extensive computations of lump solutions and their evolution within an accurate approximation of the Euler equations (which is the same model used here) indicate that certain finite amplitude lumps are stable [23].

The transverse instability of plane solitary waves (1D solitary waves trivially extended in the transverse variable) was first considered in this context in [11] using a long wave analysis, then numerically on a Kadomtsev-Petviashvilli (KP) type deep water model in [2] and on an accurate approximation to the Euler equations in [23]. Plane solitary waves are unstable for sufficiently long disturbances in the direction transverse to the propagation direction. In this paper we point out that coinciding with that instability is the emergence of a new branch of solutions, which we call *transversally periodic plane solitary waves*. These solutions are localised in the direction of propagation and periodic transversal to that direction. The study of these solutions, which are a bridge between plane waves and lumps, and their stability, through the computation of the time dependent evolution of perturbed waves, are the subject of this work. We note that the existence of transversally periodic plane solitary waves in the *shallow water* regime was proven by [9] but, to our knowledge, no such proof exists in infinite depth.

The paper is structured as follows: in §2 the classical water wave problem is presented together with its relation to the Nonlinear Schrödinger (NLS) equation. We then discuss a few results and properties of the NLS equation central to the study of GC solitary waves. In §3 the Hamiltonian truncation that we use is derived. In §4 we describe the transversally periodic profiles and bifurcation curves in parameter space. The stability of the waves as a perturbed initial value problem is examined in §5.

2. Formulation and the Nonlinear Schrödinger equation

Consider an ideal fluid under the influence of gravity in a three-dimensional domain of infinite depth and infinite horizontal extent, with a free-surface subject to capillary forces. Let (x, y) denote the horizontal plane, z the vertical direction and t time. The flow is assumed irrotational, and therefore there exists a potential function ϕ, such that the fluid velocity field $(u, v, w) = (\partial_x\phi, \partial_y\phi, \partial_z\phi)$. Denoting the displacement of the water surface by $z = \eta(x, y, t)$, the governing

equations read

$$\begin{cases} \Delta\phi + \phi_{zz} = 0 & z < \eta(x,y,t) \\ \left(\phi_x, \phi_y, \phi_z\right) \to 0 & \text{as } z \to -\infty \\ \eta_t + \eta_x\phi_x + \eta_y\phi_y - \phi_z = 0 & \text{at } z = \eta(x,y,t) \\ \phi_t + \frac{1}{2}\left[\phi_x^2 + \phi_y^2 + \phi_z^2\right] + g\eta = \frac{\sigma}{\rho}\nabla\cdot\left[\frac{\nabla\eta}{\sqrt{1+|\nabla\eta|^2}}\right] & \text{at } z = \eta(x,y,t) \end{cases} \tag{2.1}$$

where $\nabla = (\partial_x, \partial_y)^\top$ is the horizontal gradient operator, $\nabla\cdot$ is the corresponding horizontal divergent operator, and $\Delta = \partial_{xx} + \partial_{yy}$. The constants g, ρ, σ are the acceleration due to gravity, the fluid density and the coefficient of surface tension respectively. One may set these constants to one by using the space and time scales implied by the balance of surface tension and gravity as in [23].

The focussing cubic nonlinear Schrödinger (NLS) equation is central to understand the existence of GC solitary waves and some of their stability properties. These results are summarised below in the context of the current problem. NLS-based results are limited, however, by the fact that the equation describes only the small-amplitude *envelope* of the solitary wave and hence fails to capture some essential features captured by more "primitive" models such as the Hamiltonian truncation introduces in §3.

The derivation of the equation is standard [21] and follows from assuming that the free surface displacement and the potential have the prescribed asymptotic form of a slowly modulated sinusoidal carrier wave of wavelength $2\pi/k$

$$\eta(x,y,t) \sim 2\,Re\left[\epsilon A(X,Y,T)e^{ik(x-c_p(k)t)}\right] + \epsilon^2\eta_2(x,y,t) + \ldots, \tag{2.2}$$

$$\phi(x,y,z,t) \sim 2\,Im\left[\epsilon\frac{\omega}{|k|}A(X,Y,T)e^{|k|z}e^{ik(x-c_p(k)t)}\right] + \epsilon^2\phi_2(x,y,z,t) + \ldots. \tag{2.3}$$

Here, $\omega(k)$ and $c_p(k) = \omega/k$ are, respectively, the frequency and phase speed, $X = \epsilon(x - c_g t)$ is the slow modulation variable in the propagation direction, $c_g = \frac{d\omega}{dk}$ is the group speed, $4\epsilon A$ is the local crest-to-trough amplitude, $Y = \epsilon y$ is the slow variable in the transverse direction, $T = \epsilon^2 t$ a long timescale and $\epsilon \ll 1$ is a small parameter proportional to the ratio of the wavelength to a typical modulation length scale. The governing equation for the amplitude modulation is found by substituting (2.2-2.3) into (2.1) and ensuring that the solution is asymptotically valid up to order ϵ^3. This results in the 2D NLS equation

$$i\,A_T + \lambda_1\,A_{XX} + \lambda_2\,A_{YY} = \mu\,|A|^2 A, \tag{2.4}$$

The coefficients λ_1, λ_2 and μ are functions of k, the carrier wavenumber. The dispersion relation, or equivalently, the phase speed $c_p(k)$ is given by the solutions to the linearization of (2.1) about a quiescent state and is

$$c_p^2(k) = \frac{1}{|k|} + |k|.$$

The phase speed has a minimum at $k = 1$, a condition implying that phase and group speed are equal and therefore the solution (2.2) corresponds to an approximate *travelling wave* which translates without changing its shape. Under these condition, one finds that

$$c_p = \sqrt{2}, \quad \lambda_1 = \frac{\sqrt{2}}{4}, \quad \lambda_2 = \frac{\sqrt{2}}{2}, \quad \mu = -\frac{11}{8}\sqrt{2},$$

and therefore the 2D NLS equation is of the so-called *focussing* type, i.e. with $\lambda_1\mu, \lambda_2\mu < 0$. The focussing nomenclature arises from nonlinear optics, where the spatial Laplacian ($\lambda_1 = \lambda_2$) describes the effect of converging rays for an almost planar wavefront in three-dimensional space.

The well known solitary wave solution of the 1D NLS ((2.4) with $\lambda_2 = 0$): $A = a\,\mathrm{sech}(\kappa\,\mathrm{X})\mathrm{e}^{\mathrm{i}\Omega\mathrm{T}}$ with $\Omega = -\frac{1}{2}\mu a^2, \kappa = (-\mu/2\lambda_1)^{1/2}\,a$, approximates the envelope of the small amplitude *plane solitary waves* in the Euler equations [16]. The existence of transversally periodic solutions for NLS

is discussed in [3] where eigenstates of the cubic focussing NLS are obtained by setting $A = \rho e^{i\Omega T}$ and rescaling X, Y, ρ such that one may take $\lambda_1 = \lambda_2 = 1$ and $\mu = -1$. This results in the nonlinear eigenvalue problem:

$$\begin{cases} \rho_{XX} + \rho_{YY} - \rho + \rho^3 = 0 \\ \rho(X, Y + l) = \rho(X, Y), \\ \lim_{X \to \pm\infty} \rho(X, Y) = 0. \end{cases} \tag{2.5}$$

In these variables, the plane soliton solution is given by $\rho_0(X) = \pm\sqrt{2}\,\mathrm{sech}(X)$. In [3] it is shown that for the problem (2.5), there exists a one-parameter family of solutions $\rho_l(X, Y)$ for $\infty > l > 2\pi/\sqrt{3}$ which degenerate to the plane soliton solution as $l \downarrow 2\pi/\sqrt{3}$, and as l tends to infinity, become a fully localized solution with circular symmetry. This solution is the Townes' soliton, the ground state of unbounded cubic NLS, first discovered in the nonlinear optics context [5]. It was shown in [23] to approximate the envelope of fully localised lumps of the GC problem first computed in [18]. Given that both limiting cases of this NLS solution branch have counterparts in the GC problem, we should also expect the intermediate cases (i.e. transversally periodic solitary waves) in the full GC problem.

The threshold wavelength $2\pi/\sqrt{3}$ for the new branch of solutions can be obtained using a simple linear eigenvalue problem arising from a perturbation of the plane wave. Substituting the ansatz $\rho = \sqrt{2}\mathrm{sech}(X) + \alpha f(X)\cos(kY)$ into the system (2.5) and linearizing it with respect to the perturbation parameter α, one obtains:

$$f'' + 6\,\mathrm{sech}^2(X)\, f = (1 + k^2)\, f, \qquad \lim_{X \to \pm\infty} f(X) = 0 \tag{2.6}$$

This eigenvalue problem can be solved by introducing the transformation $\mu = \tanh(X)$ (see [1], pp.31), which results in the Legendre equation

$$(1 - \mu^2)\,\frac{d^2 f}{d\mu} - 2\mu\,\frac{df}{d\mu} + \left(n(n+1) - \frac{1 + k^2}{1 - \mu^2}\right) f = 0, \tag{2.7}$$

with $n = 2$. Equation (2.7) has two distinct eigenvalues which satisfy $\sqrt{1 + k^2} = 1$ and $\sqrt{1 + k^2} = 2$. The second eigenvalue gives the critical wavelength $k = \sqrt{3}$ and the corresponding eigenfunction $f = \mathrm{sech}^2(X)$ in the original coordinates.

Unsteady solutions to the NLS equation (2.4) may also be used to predict instabilities of both the plane solitary wave and the fully localised Townes' soliton. Linear stability analysis of the plane solitary wave within (2.4) (see [19]) shows that a transverse perturbation with spanwise wavenumber K_Y is unstable when the perturbation is sufficiently "long", that is,

$$0 < K_Y \leqslant \frac{\sqrt{3}}{\lambda_2} \triangleq K_c \tag{2.8}$$

This threshold coincides with the limiting wavelength of the steady nontrivial periodic state, discussed above. Furthermore, the wavenumber K_c can be used to approximate accurately a numerically verified critical wavenumber $k_c \triangleq \epsilon K_c$ for the transverse instabilities in more primitive KP type model equations of GC waves [2] and in the full problem [23]. In these papers, numerical computations show the unstable plane solitary waves focussing primarily in the transverse direction and ultimately evolving (after some dispersive radiation) into more complicated structures. These resulting structures are localised "lump" solitary waves or breathers when k_y, the transverse perturbation wavenumber, is small enough, and are transversally periodic unsteady structures when k_y is nearer k_c. In this latter case, numerical experiments in [23] showed that waves resultant from the instability were still localised in the propagation direction, but appeared to be time-periodic oscillations around a transversally periodic steadily travelling state. This is further indication that we should expect in the full GC problem *steadily* travelling free surface profiles, localised in propagation direction and nontrivially periodic in the transverse direction.

Localised steady states such as the Townes' soliton are also unstable within the 2D NLS. A virial argument (see §5) shows this, and that certain perturbations are sufficient for a focussing singularity to occur in finite time. The instabilities have been confirmed numerically also in model equations of GC waves [2] and in the full problem [23]. However, these computations do not point to the formation of singularities as does NLS. The focussing instability is arrested with the formation of apparently stable oscillatory breather-like structures. In addition to these breathers, steadily travelling larger amplitude "lumps" were also found and observed to be *stable*.

In what follows we complete the picture of CG travelling structures in the GC problem by numerically computing the transversally periodic states from their emergence at k_c to their limiting lump configuration. We discuss both small amplitude cases where the waves' envelopes are well described by the NLS equation and larger amplitude solutions, which differ considerably from those. The stability of the computed structures is tested through time evolution of perturbed initial states.

3. Hamiltonian Formulation and Truncation

In this section we sketch the reformulation of the water wave problem into Hamiltonian form (first introduced by Zakharov [24]) and present the truncated approximation that we shall use subsequently in the paper. The principal ingredients are the introduction the surface potential $\xi(x,y,t) \triangleq \phi(x,y,\eta(x,y,t),t)$ and the (scaled) Dirichlet to Neumann operator

$$G(\eta)\,\xi \triangleq \sqrt{1+(\nabla\eta)^2}\,\phi_n.$$

A Dirichlet to Neumann operator maps Dirichelet data ξ to the normal derivative of ϕ, $\phi_n(x,y,\eta(x,y,t),t)$ on the free surface given a *particular* fluid domain defined by $\eta(x,y,t)$. It is a nonlocal operator, linear in ξ and nonlinear in η, that could in principle be evaluated by solving for the velocity potential $\phi(x,y,z,t)$ in the the entire domain *given* Dirichelet data and then computing its normal derivative on the free boundary. Instead of this, we shall use an expansion of this operator about G_0, the easily found form for a horizontal free surface [7]. In fluid dynamics terms, the Dirichelet to Neumann operator can be thought of as a inducing a map between the tangential and normal velocities at the free surface. The scaling factor of $\sqrt{1+(\nabla\eta)^2}$ arises from the kinematic boundary condition whereby

$$\eta_t = \left(\phi_z - \nabla\eta\cdot\nabla\phi\right)_{z=\eta} = \sqrt{1+(\nabla\eta)^2}\,\phi_n$$

Henceforth, we shall use the term "Dirichlet to Neumann operator" to mean the operator that includes this scaling.

The Hamiltonian, which is the total physical energy of the system, can be expressed as

$$\begin{aligned}\mathcal{H}[\eta,\xi] &= \frac{1}{2}\int dxdy\int_{-\infty}^{\eta}\left(\phi_x^2+\phi_y^2+\phi_z^2\right)dz+\frac{1}{2}\int\eta^2\,dxdy\\ &\quad+\int\left(\sqrt{1+\eta_x^2+\eta_y^2}-1\right)dxdy\\ &= \frac{1}{2}\int\left[\xi G(\eta)\xi+\eta^2+2\left(\sqrt{1+\eta_x^2+\eta_y^2}-1\right)\right]dxdy \qquad (3.1)\end{aligned}$$

In the expression above the first term is the kinetic energy of the fluid, the second term is the gravitational potential energy and the last term is the surface energy due to capillary effects. The evolution of the system is given by the kinematic and dynamic boundary conditions (the last two equations in (2.1)) which can be obtained from the variational derivatives with respect to the

canonically conjugate variables ξ and η:

$$\eta_t = \frac{\delta \mathcal{H}}{\delta \xi} = G(\eta)\xi \tag{3.2}$$

$$\xi_t = -\frac{\delta \mathcal{H}}{\delta \eta} = \frac{1}{2(1+|\nabla\eta|^2)}\Big[(G(\eta)\xi)^2 - |\nabla\xi|^2 + 2(G(\eta)\xi)\nabla\xi\cdot\nabla\eta - |\nabla\xi|^2|\nabla\eta|^2 + (\nabla\xi\cdot\nabla\eta)^2\Big] - \eta + \nabla\cdot\left[\frac{\nabla\eta}{\sqrt{1+|\nabla\eta|^2}}\right] \tag{3.3}$$

This formulation reduces the three-dimensional problem to a two-dimensional one, but with the complication of introducing the nonlocal and unknown Dirichlet to Neumann operator.

A simplification arises by writing the Dirichlet to Neumann operator using an expansion $G(\eta) = \sum_{i=0}^{\infty} G_i(\eta)$, where G_i is of degree i in η. For infinite depth, the first three terms of the series are given by [7]

$$G_0(\eta) = (-\Delta)^{1/2},$$

$$G_1(\eta) = -G_0\cdot\eta G_0 - \nabla\cdot\eta\nabla,$$

$$G_2(\eta) = \frac{1}{2}\Delta\eta^2 G_0 + \frac{1}{2}G_0\eta^2\Delta + G_0\eta G_0\eta G_0.$$

G_0 is the Dirichelet to Neumann operator for a half-space in $\mathbb{R}^3$. It is most easily evaluated in Fourier space since the solution to Laplace's equation can be written as $\hat{\phi}(x,y,z,t) = e^{|\mathbf{k}|z}\hat{\phi}(x,y,0,t)$ where $\hat{\cdot}$ denotes the Fourier transformed function and $\mathbf{k} = (k_x, k_y)$ are the Fourier transform variables. Therefore, $\hat{\phi}_n = \hat{\phi}_z(x,y,0,t) = |\mathbf{k}|\hat{\phi}(x,y,0,t) = |\mathbf{k}|\hat{\xi}$, showing that the Fourier symbol of G_0 is $|\mathbf{k}|$, which can be taken as the definition of $(-\Delta)^{1/2}$.

Here, we approximate the Hamiltonian using a three-term truncation of G which has been previously verified numerically for accuracy in [23]. Thus,

$$\mathcal{H} = \frac{1}{2}\int\Big[\xi\big(G_0+G_1+G_2\big)\xi + \eta^2 + 2\Big(\sqrt{1+\eta_x^2+\eta_y^2}-1\Big)\Big]\,dxdy + \mathbb{O}\big(|\eta|^3|\xi|^2\big) \tag{3.4}$$

$$\triangleq \mathcal{H}_T + \mathbb{O}\big(|\eta|^3|\xi|^2\big), \tag{3.5}$$

and we now use $\mathcal{H}_T$ and take variational derivatives as in (3.2) and (3.3), to obtains a simpler system, used in the remainder of the paper, for the evolution of free surface displacement and surface potential:

$$\eta_t - G_0\xi = \big(G_1+G_2\big)\,\xi \tag{3.6}$$

$$\xi_t + (1-\Delta)\eta = \frac{1}{2}\Big[\big(G_0\xi\big)\big(G_0\xi - 2G_0\eta G_0\xi - 2\eta\Delta\xi\big) - |\nabla\xi|^2\Big] + \nabla\cdot\left[\frac{\nabla\eta}{\sqrt{1+|\nabla\eta|^2}} - \nabla\eta\right] \tag{3.7}$$

Similar truncations have been used in the past, first by Craig & Sulem [7] for the numerical simulation of pure gravity waves, and for example in [17], where this method was first used to seek travelling waves. The present formulation, however, differs importantly from prior cases where the truncation of Dirichlet to Neumann operator was made in the primitive equations (3.2) and (3.3) instead of the Hamiltonian (3.1), leading to a difference in the kinematic evolution equation and a loss of Hamiltonian structure. For GC waves the Hamiltonian model (3.6-3.7) agrees remarkably well with the full potential equations for the bifurcation curves, wave profiles and the dynamics of solitary waves for a two-dimensional fluid domain, and with higher-order truncations of the Hamiltonian in three dimensions [23]. In the next section we make a brief comparison between the Hamiltonian truncation and the truncations of the primitive equations (such as those in [7] and [17]).

Finally, we note that a fourth order Hamiltonian truncation, leading to evolution equations accurate to cubic order, is the lowest order model that can capture effects also captured by NLS (which is itself cubic). Indeed the NLS equation that can be derived from (3.6-3.7) is *identical* to the one derived from the full equations (2.1). However, the model (3.6-3.7) contains far more dynamical effects (for example, all resonant triads and quartets are captured exactly) and should thought of as a good approximation to the full potential flow equations up to moderate amplitudes [23].

In the following section we describe travelling wave solutions to the fluid system (3.6)-(3.7) using, in part, the NLS solutions of §2 to construct approximate initial guesses at small amplitude.

4. Travelling waves

The small amplitude 1D CG problem in the Euler equations has "elevation" and "depression" travelling solitary waves corresponding to whether the midpoint of the (symmetric) wave is above or below the mean free surface elevation [22]. This feature is not predicted by the 1D NLS equation, as it describes only the envelope of the wave, and elevation and depression waves differ by π in the relative phase between the envelope and the carrier wave. In fact, the NLS equation predicts a continuous family of waves with arbitrary relative phase between 0 and π. The transversally periodic solitary waves presented below are found to be also of elevation or depression type (indicated by the sign of $\eta(0,0)$ in the figures). For the same reasons given above, this could not have been predicted by the 2D NLS equation.

Steady solutions to equations (3.6-3.7) are sought in a frame of reference translating at an unknown speed c in which the solution is steady. Assuming η and ξ are periodic functions of $x-ct$ and y with periodicity of L and $2\pi/k_y$ respectively, we expand

$$\eta = \sum_{m=0}^{M}\sum_{n=0}^{N} a_{mn}\cos\left(m\frac{2\pi}{L}(x-ct)\right)\cos(nk_y y), \tag{4.1}$$

$$\xi = \sum_{m=0}^{M}\sum_{n=0}^{N} b_{mn}\sin\left(m\frac{2\pi}{L}(x-ct)\right)\cos(nk_y y), \tag{4.2}$$

with $a_{00}=b_{00}=0$. Inserting into (3.6)-(3.7), the resultant nonlinear algebraic system for the Fourier coefficients and c is solved using Newton's method. The nonlocal operator G_0 and derivatives are obtained by using the Fourier multipliers, while nonlinear terms are computed pseudo-spectrally in physical space. The solution branches in the bifurcation diagrams are computed using either c or k_y as continuation parameters. L is fixed sufficiently large for the solution to approximate a localised disturbance in x (this is checked by increasing L and observing that the solution does not change appreciably). In most computations, 256×64 grid points are used along the propagating and transverse directions respectively. Two types of initial guesses were used: either the fully localised solitary wave solutions found in [23] for which the period in the y direction is gradually decreased (k_y is increased) to obtain the periodic wave profiles, or monochromatic waves modulated by the transverse-periodic solitons to the cubic NLS equation.

We begin with a comparison of the errors between solutions found using the different truncations mentioned in §3 and those of the full potential flow equations for a one dimensional free surface case (i.e. plane waves) where accurate solutions to the full equations are available ([22], [16]). Figure 1 (left panel) shows two examples of the depression plane wave profile at small and large amplitudes. Figure 1 (right panel) shows the relative maximum pointwise error in the free-surface displacement for waves of depression, for a range of speeds. The solutions were found using the Fourier method described above, simplified to one-dimension, for various models: the fourth-order Hamiltonian truncation resulting in (3.6-3.7), a sixth-order Hamiltonian truncation, and third- and fifth-order truncations of the primitive equations as proposed in [7] and [17]. (From the symmetries of the problem odd-order truncations in the evolution equations, and even order Hamiltonians are preferable.) It is clear that over a large range of wave speeds

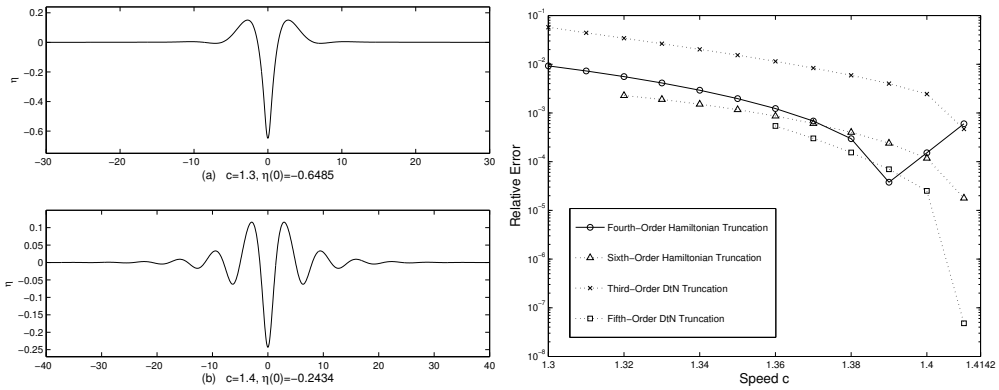

Figure 1. Left: cross sectional profiles of small and large amplitude plane waves. Right: relative error of various truncation methods when compared to the full Euler equations. The present truncation (solid line) has errors below 1% over a broad range of amplitudes.

corresponding to a large range of amplitudes, the quartic Hamiltonian is approximately an order of magnitude more accurate than the formally equivalent primitive equation cubic truncation. Furthermore, higher order truncations of both types are far more delicate to use computationally, and we were unable to make those solutions converge over the full range of speeds in the figure.

In Figure 2 a typical small amplitude depression solitary-periodic wave free-surface profile is shown. This example corresponds to a wave near the secondary bifurcation shown in Figure 5. As expected from their form as described by the NLS equation, they appear as a sinusoidal carrier wave (evidenced by the fast oscillation in x of period approximately 2π corresponding to $k = 1$) which is slowly modulated by an envelope of the form $2\epsilon(\mathrm{sech}(\epsilon x) + \alpha\,\mathrm{sech}^2(\epsilon x)\cos(\epsilon K_y y))$ where ϵ is a measure of the amplitude and α is a measure of the distance from the secondary bifurcation point. Hence, the travelling waves have a fast oscillation decaying in the direction of propagation and have a slow periodic modulation in the direction perpendicular to propagation. Figures 3 and 4 show larger amplitude depression and elevation waves with the same transverse modulation period as in Figure 2 (i.e. waves further along the secondary bifurcation branch shown in Figure 5). These waves are more localised in space than the wave in Figure 2. The principal difference between elevation and depression waves is that the former has two pronounced troughs, whereas the latter has only one.

We now turn to bifurcation curves. Several parameters are used to show the solution branches: the wave speed c, the transverse wavenumber k_y, and three measures for the amplitude. The amplitude measures are the free-surface displacement at the origin $\eta(0,0)$, which is traditionally used as a bifurcation parameter ([22], [18]), and two physical energies:

$$E(c,k_y) = \frac{1}{2}\int_{-\pi/k_y}^{\pi/k_y} dy \int_{-\infty}^{\infty} dx \left[\xi\big(G_0+G_1+G_2\big)\xi + \eta^2 + 2\Big(\sqrt{1+\eta_x^2+\eta_y^2}-1\Big)\right]$$

and $e(c,k_y) = \frac{k_y}{2\pi}E$. E is the total energy over a transversal period of the wave and e is the average energy per transversal unit length. These energies are more useful amplitude parameters than surface displacement as they yield stability information (see §5). Both energies are needed because, in the limit of plane solitary waves, E is infinite but e is finite, whereas, in the limit of fully localised waves, e is zero but E is positive.

The NLS equation may be used to predict the largest unstable transverse wavenumber as a function of the amplitude of the plane solitary waves. Or, for a given transverse wavenumber, the amplitude of the plane wave required for the onset of the secondary bifurcation at which

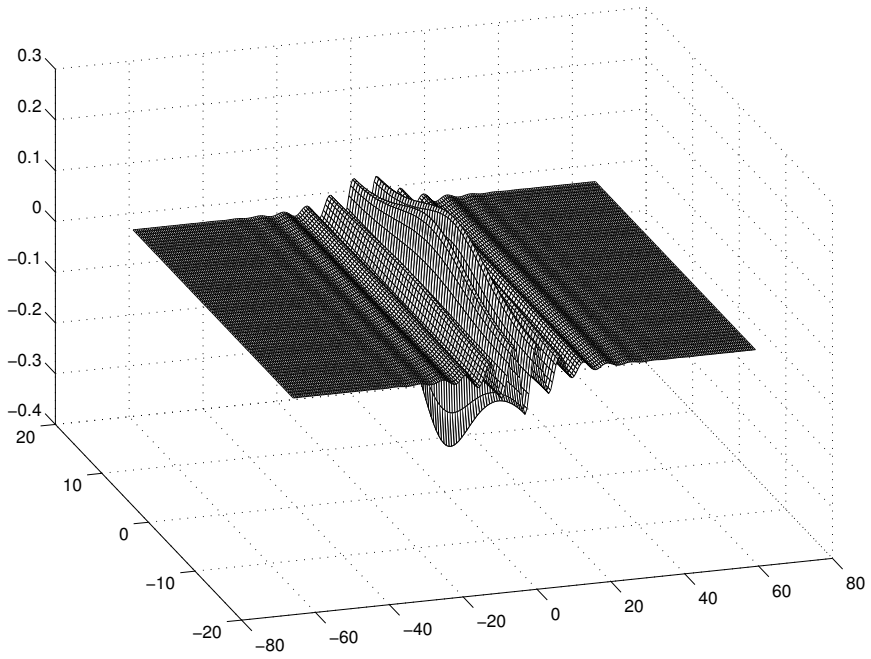

Figure 2. Typical profile of a small amplitude transverse-periodic depression solitary wave. $k_y = 0.18$, Energy = 6.7, c = 1.405, $\eta(0,0) = -0.305$.

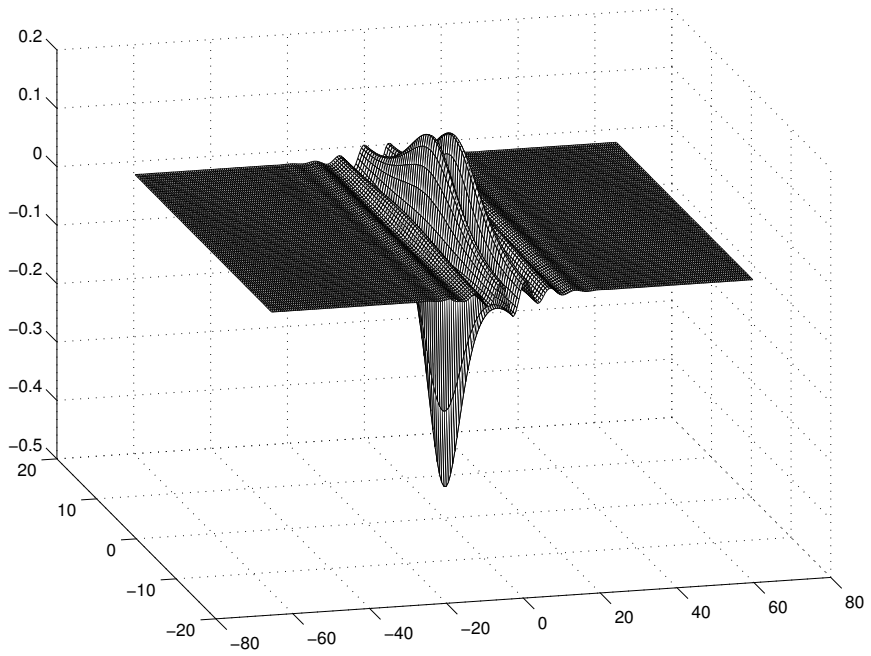

Figure 3. Typical profile of a larger amplitude transverse-periodic depression solitary wave. $k_y = 0.18$, Energy = 6.7, c = 1.392, $\eta(0,0) = -0.466$. Note that this wave has the same energy *and* transverse period as that of Figure 2. This wave is therefore to the left of the minimum of the speed-Energy curve and is stable (see §5), while the wave in Figure 2 is unstable.

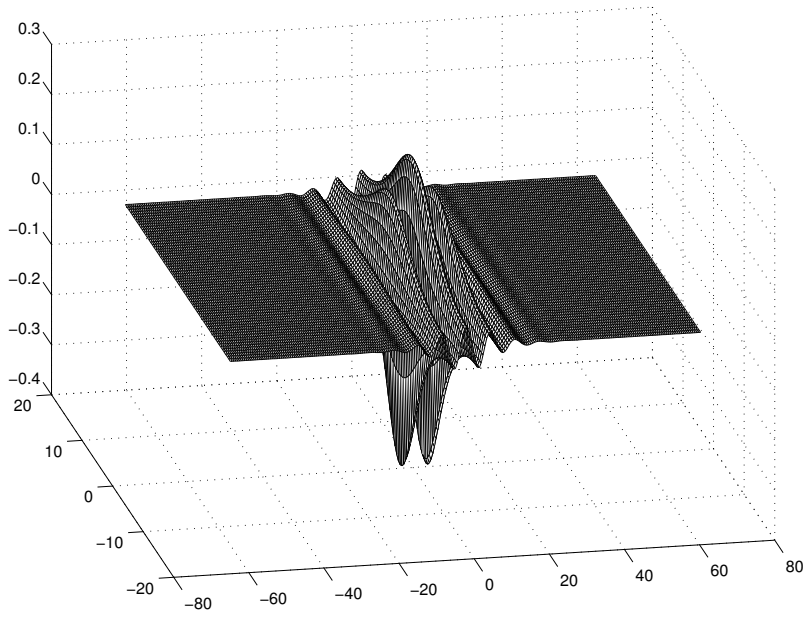

Figure 4. Typical profile of a larger amplitude transverse-periodic elevation solitary wave. $k_y = 0.18$, Energy = 13.18, c = 1.391, $\eta(0,0) = 0.218$.

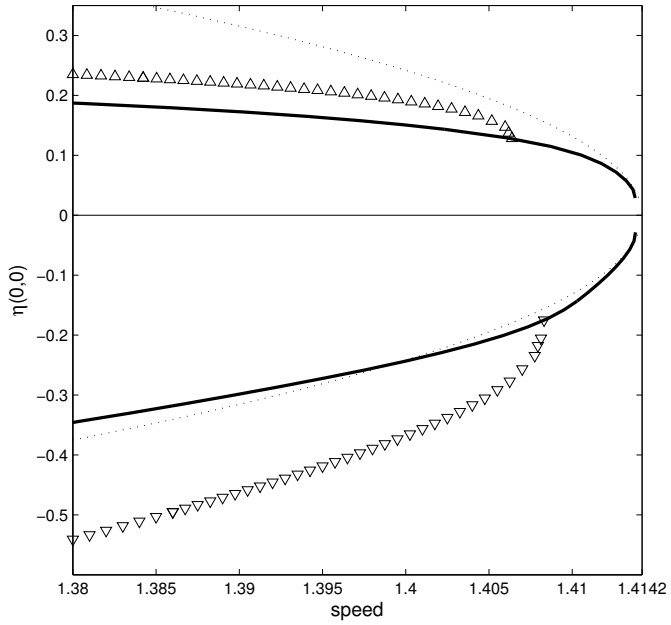

Figure 5. Speed-amplitude bifurcation curves for elevation (up triangles) and depression (down triangles) transversally periodic solitary waves for $k_y = 0.18$. The solid lines correspond to the plane waves of the system bifurcating from $c = \sqrt{2}$. The dotted lines are the NLS predictions for these plane waves

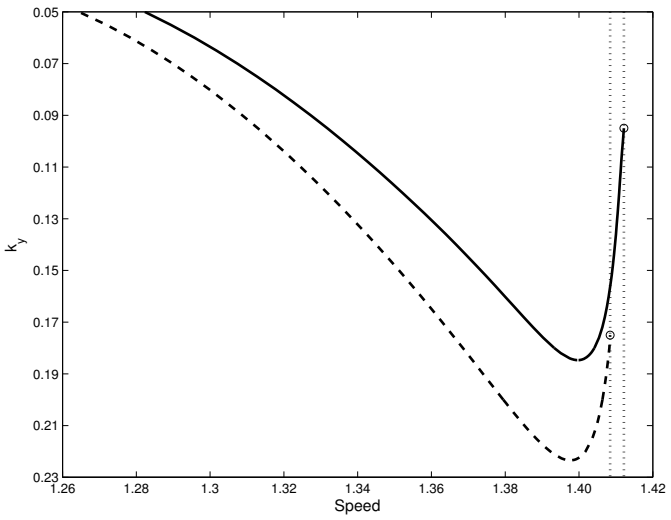

Figure 6. Bifurcation curves for depression transversally periodic solitary waves for fixed energy density e. The solid line corresponds to $e = 0.19$ and the dashed line to $e = 0.24$. The dotted lines corresponds to the plane solitary wave. According to numerical experiments in §5, when subject to small perturbations of transverse periodicity $2\pi/k_y$, the waves to the right of the minimum are unstable and those on the left, stable.

transversally periodic waves arise. From the relations $K_c = \epsilon k_c = \sqrt{3}/\sqrt{\lambda_2}$ and $||\eta||_\infty = 2\epsilon A$,

$$k_c = \sqrt{\frac{33}{32}}\,||\eta||_\infty. \tag{4.3}$$

This prediction is quite accurate for depression waves: in the cases shown in Figures 5 and 6, $k_c = 0.095, ||\eta||_\infty = |\eta(0,0)| = 0.0982$ and $k_c = 0.175, |\eta(0,0)| = 0.174$. For elevation waves, the agreement is less good, for example, for the elevation branch in Figure 5, $k_c = 0.18, , |\eta(0,0)| = 0.128$.

Figure 5 shows the bifurcation diagram in the $c - \eta(0,0)$ plane for both elevation and depression plane waves and transverse periodic waves at a fixed value of k_y. If a k_y is varied, the location of the secondary bifurcation will slide along the plane wave branch. The curves for the 1D NLS plane wave prediction are also shown for comparison. Note that (i) the transversally periodic waves are a secondary bifurcation from *finite amplitude* plane waves and have speeds strictly smaller than the speed at which planes waves bifurcate from the undisturbed state, $c = \sqrt{2}$ (which in turn is the minimum speed of linear GC waves); (ii) elevation and depression waves of the same transverse period bifurcate at different speeds - a feature that is not accurately described by the NLS approximation (4.3) which does not distinguish between elevation and depression branches.

Figure 6 shows the solution curves for fixed energy density e in the $k_y - c$ plane for depression waves. The dashed lines correspond to the plane wave at the same value of e. Note that the branches are subcritical: near bifurcation, as the speed decreases, the wavenumber increases first (i.e. there exists shorter transverse period waves of the same energy) before decreasing to zero in the limit of fully localised waves (which are not shown in the figure since they have zero energy density).

Figure 7 shows the bifurcation diagram at fixed k_y in the $E - c$ and $e - c$ planes. The energy density e, used on the left panel is appropriate to compare transversally periodic solutions to plane waves (solid lines) whereas the total energy E over a period used on the right panel is appropriate for comparison with fully localised "lump" solutions which always have finite total

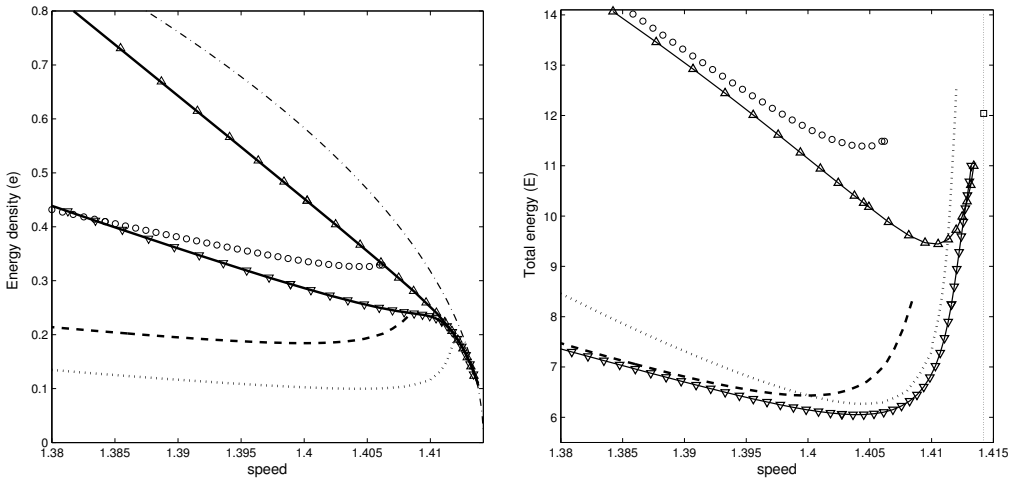

Figure 7. Bifurcation curves for depression and elevation transversally periodic solitary waves for fixed transversal wavenumber k_y. In both figures, dashed and dotted curves correspond to transversally periodic depression solitary waves with $k_y = 0.18$ and $k_y = 0.1$ respectively. Circles correspond to transversally periodic elevation solitary waves with $k_y = 0.18$. Left: Energy density e versus speed. Solid lines with up and down triangles correspond to plane solitary waves of elevation and depression respectively. The dash-dot line is the 1D NLS prediction for plane waves. Right: Total energy per period E versus speed. Solid lines with up and down triangles correspond to fully localised lump solitary waves of elevation and depression respectively. The square is the 2D NLS prediction of the Townes' soliton for which $E = 12.04$ [23].

energy (even at bifurcation) but zero energy density. The lump solutions are the lowest energy state for all k_y and speeds.

From these figures one can make the following conjectures about the stability of transverse periodic solitary waves (when subject to perturbations of the same basic transverse period): (i) elevation waves are unstable as their energy levels are much larger than depression ones. (Some 1D large amplitude elevation plane waves are stable [4] but they are beyond the regime considered here.) (ii) Depression waves are unstable near their bifurcation point as, for fixed wavenumber, the energy of the wave decreases as the speed decreases. (iii) Depression waves change stability at the minima of the speed-energy curves, and are stable to the left of the minima (i.e. at lower speeds) in agreement with what is observed for lumps [23]. In addition, *finite-amplitude* instabilities of plane waves occurring due to the subcritical nature of the bifurcation of transversally-periodic waves (see Figure 6) are expected. Hence sufficiently large perturbations with wavenumber *larger* than k_c, will destabilise the plane wave, a feature not captured by linear stability analysis. These conjectures are supported by the numerical experiments shown in the following section.

5. Time-dependent solutions and stability

In this section the stability of transversally-periodic traveling waves is investigated through numerical experiments of the time-dependent equations. While the results in this section are only show a small number of dynamical experiments with particular initial conditions, our observations are that the behaviour is qualitatively representative of the dynamics for a large class of perturbations of travelling waves.

In all experiments presented, numerical time integration of the system (3.6-3.7) is performed using a Fourier spectral method described in [23]. Briefly, defining $\hat{p} = \hat{\eta} + i|\mathbf{k}|/\hat{\mathcal{L}}(\mathbf{k})\hat{\xi}$ where $\hat{\mathcal{L}} =$

$\sqrt{|\mathbf{k}|(1+\mathbf{k}^2)}$, the system can be written as a single complex equation

$$\hat{p}_t + i\hat{\mathcal{L}}\hat{p} = \hat{\mathcal{N}}(\hat{p}),$$

where $\mathcal{N}$ includes all the nonlinear terms. The system is now discretized using a finite set of Fourier modes

$$\hat{p} = \sum_{m=-M/2}^{M/2} \sum_{n=-N/2}^{N/2} p_{mn}(t) e^{im\frac{2\pi}{L_x}x} e^{in\frac{2\pi}{L_y}y},$$

and it is the the evolution of $p_{mn}(t)$ is computed. The linear evolution can be integrated exactly see [15] for details) and the nonlinear terms $\mathcal{N}$ are computed in a combination of real and Fourier space for efficiency. Half-mode de-aliasing is used in nonlinear terms throughout our computations, and a fourth order Runge-Kutta scheme is used for time integration.

There are two relevant analytical results that guide the computations. First we may expect a linear change of stability at extrema of $\mathcal{H}_T(c)$ (or equivalently $E(c)$) curve, a necessary condition for the change of stability of a neutral mode arising from the translational invariance of the problem [20]. The second result is the focussing or defocussing behaviour of NLS (see, for example, [21]). This result has been proven only for fully localised data, and states that, for the normalised NLS (2.4) with $\lambda_1 = \lambda_2 = \mu = 1$, if the Hamiltonian

$$\mathcal{H}_N = \int |\nabla A|^2 - \frac{1}{2}|A|^4,$$

is initially negative, the solution will focus (i.e. $|A|^2$ will concentrate while $\int |A|^2$ is preserved) to a singularity in finite time. For the opposite sign, the solution "defocusses": $\int (X^2+Y^2)|A|^2$ increases without bound, and the wave disperses away. The Townes soliton, and the transverse periodic NLS solutions satisfying (2.5) have $\mathcal{H}_N = 0$ (where, in the case of transverse periodic waves, is defined over a period).

Firstly, we consider initial conditions of the form

$$\eta = (1+\epsilon)\,\eta_0(x,y,c) \tag{5.1}$$

where η_0 denotes the elevation or depression transverse periodic solutions found in the previous section, and ϵ is a small parameter that determines the amplitude and sign of the perturbation. Whilst a focussing argument similar to the one above has not been proven for the periodic case, in our limited experiments the result holds qualitatively for depression solitary waves in the small amplitude regime (i.e. solutions to the right of the minimum in the Figure 7). An example of this is shown in Figure 8(a) where we tracked the maximum amplitude of the free surface arising from perturbed initial data of the form (5.1). When $\epsilon > 0$, and therefore $\mathcal{H}_N < 0$, there is an initial focussing instability resulting in large growth. What follows is a recurrent finite-amplitude oscillatory travelling state: a transversally periodic breather type solution similar to those found in the unbounded case by [23]. A typical example of such a recurrent state is shown in the bottom two panels of Figure 9 which correspond to the minimum and maximum amplitude of a similar state arising from a different instability. Using the same travelling solution η_0, but taking $\epsilon < 0$ yields the other curve in Figure 8(a). Now, the wave defocuses and the amplitude decreases in magnitude until the periodic domain is filled with linear waves.

When η_0 is chosen to have larger amplitude (i.e. solutions beyond the regime approximated by the NLS and to the left of the minimum in Figure 7) the transverse periodic waves appear to be numerically stable. This is shown in Figure 8(b) where, independently of the sign of ϵ, the solution remains close to the original travelling wave.

All elevation transverse-periodic waves that we tested were unstable. A typical example of the evolution of an elevation wave similar to that of Figure 4 perturbed as in (5.1) is shown in Figure 9. The solution which initially has two deep troughs (see Figure 4) experiences an instability whereby the rear trough deepens at the expense of the forward one, releasing a linear radiated wave field ahead. The newly formed structure is similar to a depression wave and focusses into a depression breather, much like the one present after the focussing instability of small amplitude

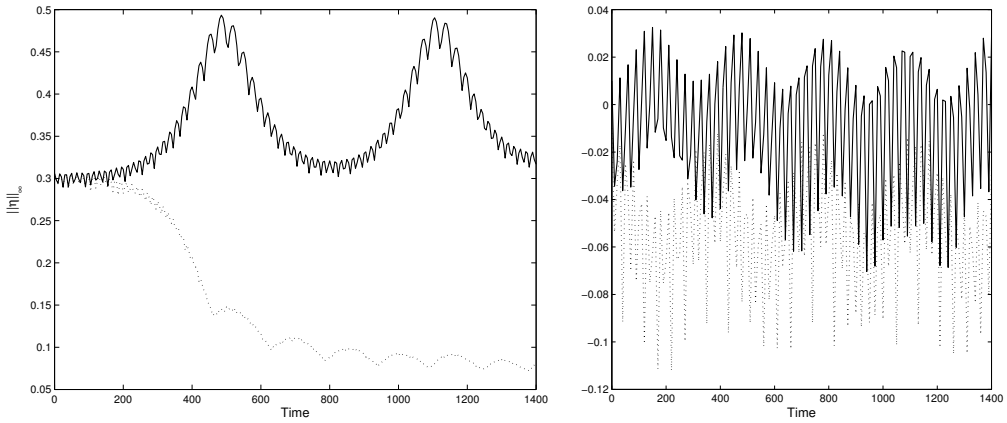

Figure 8. (a) Evolution of the maximum norm (trough depth) for perturbed depression waves in the small-amplitude regime ($c = 1.4047$, $energy = 6.7074$ and $\eta(0,0) = -0.3054$). Solid line, positive amplitude perturbation ($\epsilon = 0.002$); dashed line, negative amplitude perturbation ($\epsilon = -0.002$). (b) Evolution of maximum trough depth (departure from unperturbed trough depth) for depression waves in the moderate-amplitude regime ($c = 1.3927$, $energy = 6.6591$ and $\eta(0,0) = -0.4391$). Solid line, positive amplitude perturbation ($\epsilon = 0.01$); dashed line, negative amplitude perturbation ($\epsilon = -0.01$).

depression waves. Figure 9 shows this evolution in four snapshots: the first two corresponding to the initial stage of the deepening rear trough, and the lower two showing two frames separated by a half-period of the periodic pulsation.

As alluded in the previous section, our bifurcation curves (see Figure 6) also point to the possibility of a *finite-amplitude* instability of the *plane waves* for perturbations with transverse periods shorter than that predicted by NLS. A typical example is shown in Figure 10. The initial data for these set of experiments has the form

$$\eta = (1 + \epsilon \cos(k_y y))\, \eta_0(x, c) \tag{5.2}$$

where $\eta_0(x, c)$ is a plane depression solitary wave. If $k_y > k_c$ given by (4.3) the weakly nonlinear stability analysis predicts stability (see, for example, [11]), which is confirmed numerically. However, larger perturbations of the same transverse wavenumber destabilise the plane wave. In this case, the long time evolution is, once more, dominated by a transverse periodic depression breather.

6. Conclusion

Gravity-capillary free surface flows support a variety of solitary waves. Here we found that there exist travelling two-dimensional surface profiles that are localised in the travelling direction and are periodic in the transverse one. These transverse periodic solitary waves are either of elevation or depression type, and the depression waves along this branch connect two limiting cases: plane solitary waves and fully localised lumps. The stability properties of these waves are considered through time dependent computations.

All solitary waves are found to be unstable, except depression waves whose amplitude is above a critical value. These stable waves, together with transverse periodic *breathers* that appeared consistently in instability calculations, act as attractors in the time evolution of the system for a broad class of initial data. In the dynamics leading to these attractors, dispersive radiation plays the role of dissipation in the formation of the breathers. The resilience and universality of these breathers is a surprising outcome of this work.

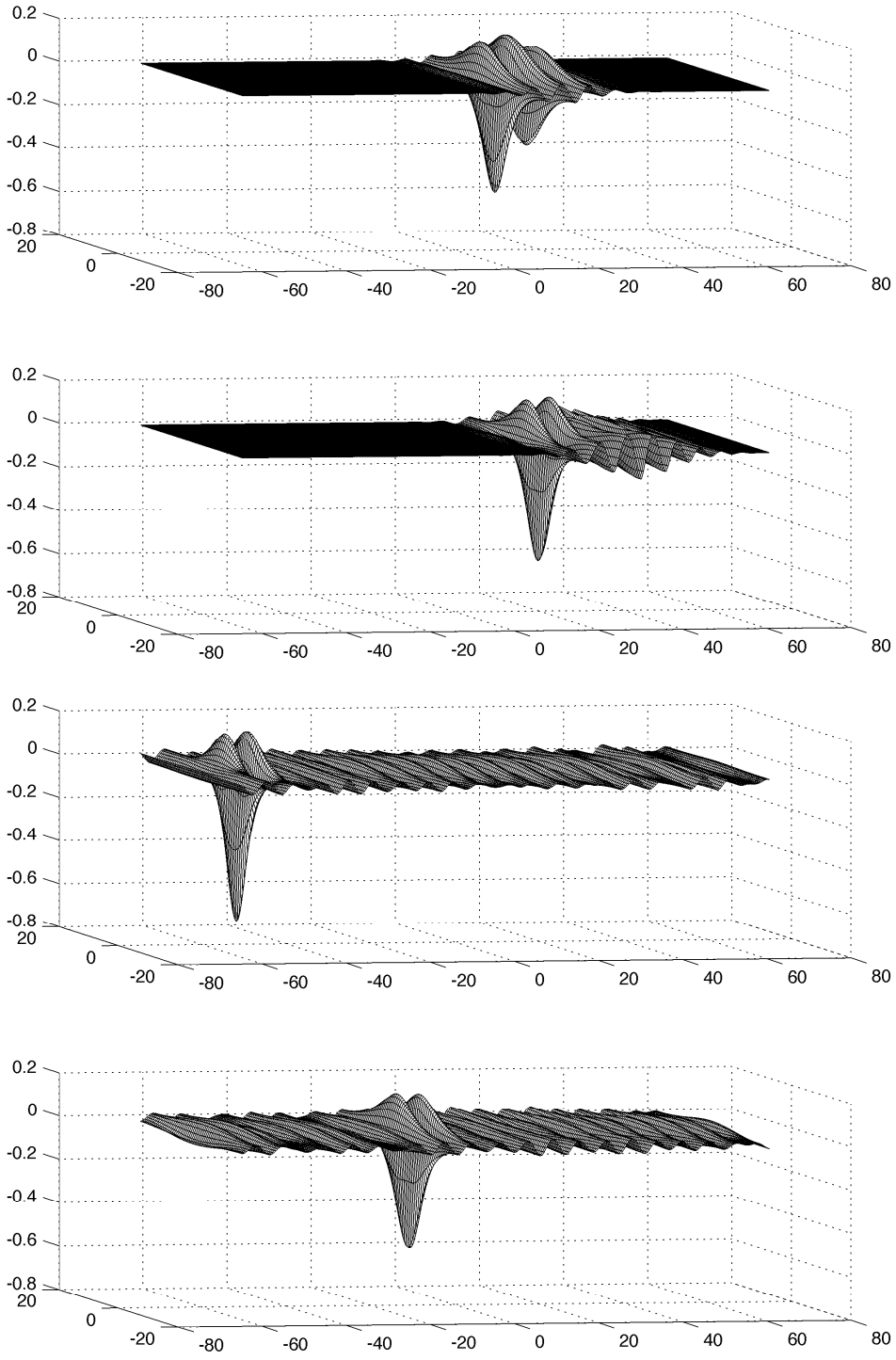

Figure 9. Four snapshots of the evolution of a moderate-amplitude unstable elevation wave with $c = 1.3995$, $\eta(0,0) = 0.193$. The initial wave is similar to that of Figure 4. The initial data was constructed as in (5.1) with $\epsilon = -0.002$. The evolution leads to a depression breather and small amplitude waves radiated during the instability. The solution is shown at time 190 and 290 where the initial instability takes place, and then 790 and 820 which correspond approximately to the times of maximum and minimum amplitudes of the periodic breather motion.

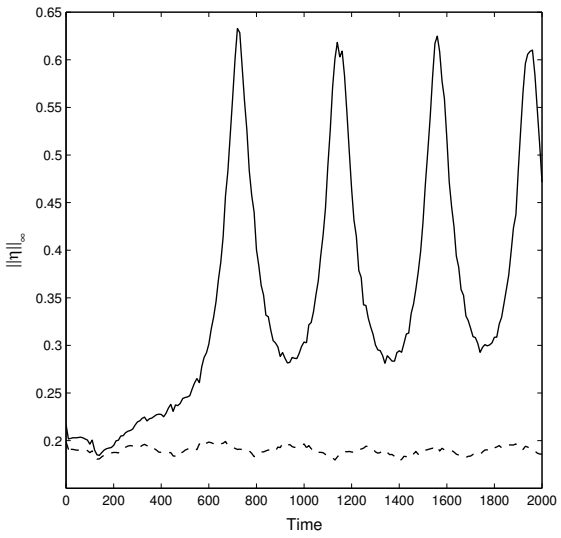

Figure 10. Stability and instability for the same plane solitary wave with different perturbations. A plane solitary wave with trough depth -0.1806 and $c = 1.4084$ was subject to perturbations as in (5.2) with $k_y = 0.195$ and $\epsilon = 0.1$ (dashed line) or $\epsilon = 0.2$ (solid line). The former perturbation does not trigger an instability while the latter does.

Througout this work we have used a truncated version of the free surface fluid equations. While we have demonstrated its accuracy in the waves computed here, truncations of any order have serious limitations. Calculations of complicated structures such as overhanging waves (see for example [22]) cannot be studied using these methods and require a different formulation.

We believe that the new waves, and the dynamical effects described here, could be an important ingredient in understanding the energy transfer due to wind forcing of capillary-gravity ripples. All the structures described in the paper exist in a regime *below* the minimum speed of linear waves, and therefore may be the first excited modes for low wind speeds. This would imply that linear theories would underestimate energy transfer. A reasonable model for wind forcing must also include dissipation, since, in the length scales considered here, dissipative timescales can be estimated to be similar to the timescale observed in the focussing instability [23].

Acknowledgment

This work was supported by EPSRC, under grant nos. EP/J019569/1 (Z.W.) and EP/J019321/1 (P.A.M.) and by a Royal Society Wolfson award (P.A.M.).

References

1. Ablowitz MJ, Clarkson PA. 1991 *Solitons, Nonlinear Evolution Equations and Inverse Scattering*. London Mathematical Society Lecture Note Series, Vol. 149, Cambridge University Press.
2. Akers B, Milewski PA. 2009. A model equation for wavepacket solitary waves arising from capillary-gravity flows. *Stud. in Appl. Math.*, **122**, 249–274.
3. Alfimov GL, Eleonsky VM, Kulagin NE, Lerman LM, Silin VP. 1990. On existence of non-trivial solutions for the equation $\Delta u - u + u^3 = 0$. *Physica D*, **44**, 168–177.
4. Calvo DC, Yang TS, Akylas TR. 2002. Stability of steep gravity-capillary waves in deep water. *J. Fluid Mech.*, **452**, 123–143.
5. Chiao RY, Garmire E, Townes C. 1964. Self-trapping of optical beams. *Phys. Rev. Lett.*, **13**, 479–482.

6. Coantic, M. 1986. A model of gas transfer across air-water interfaces with capillary waves. *J. Geophys. Res. C*, **91**, 3925–3943.
7. Craig W, Sulem C. 1993. Numerical simulation of gravity waves. *J. Comp. Phys.*, **108**, 73–83.
8. Dias F, Menasce D, Vanden-Broeck JM. 1996. Numerical study of capillary-gravity solitary waves. *Eur. J. Mech., B/Fluids*, **15**, 17–36.
9. Groves MD, Haragus M, Sun SM. 2002. A dimension-breaking phenomenon in the theory of steady gravity-capillary water waves. *Phil. Trans. R. Soc. Lond. A*, **360**, 2189–2243.
10. Kim B, Akylas TR. 2005. On gravity-capillary lumps. *J. Fluid Mech.*, **540**, 337–351.
11. Kim B, Akylas TR. 2007. Transverse instability of gravity-capillary solitary waves. *J. Eng. Math.*, **58**, 167–175.
12. Longuet-Higgins MS. 1989. Capillary-gravity waves of solitary type on deep water. *J. Fluid Mech.*, **200**, 451–478.
13. Makin VK, Kudryavtsev VN. 1999. Coupled sea surface-atmosphere model: 1. Wind over waves coupling. *J. Geophys. Res. C*, **104**, 7613–7623.
14. Milewski PA. 2005. Three-dimensional localized gravity-capillary waves. *Comm. Math. Sci.*, **3**, 89–99.
15. Milewski PA, Tabak EG. 1999. A pseudospectral procedure for the solution of nonlinear wave equations with examples from free-surface flows. *SIAM J. Sci. Comput.*, **21(3)**, 1102–1114.
16. Milewski PA, Vanden-Broeck JM, Wang Z. 2010. Dynamics of steep two-dimensional gravity-capillary solitary waves. *J. Fluid Mech.*, **664**, 466–477.
17. Nicholls DP. 1998. Traveling water waves: spectral continuation methods with parallel implementation. *J. Comp. Phys.*, **143**, 224–240.
18. Părău EI, Vanden-Broeck JM, Cooker MJ. 2005. Nonlinear three-dimensional gravity-capillary solitary wave. *J. Fluid Mech.*, **536**, 99–105.
19. Rypdal K, Rasmussen JJ. 1989. Stability of solitary structures in the nonlinear Schrödinger equations. *Physica Scripta*, **40**, 192–201.
20. Saffman PG. 1985. The superharmonic instability of finite amplitude water waves. *J. Fluid Mech.*, **159**, 169–174.
21. Sulem C, Sulem PL. 1999 *The Nonlinear Schrödinger Equation: Self-Focussing and Wave Collapse.* Applied Mathematical Science, Vol. 139, Springer.
22. Vanden-Broeck JM, Dias F. 1992. Gravity-capillary solitary waves in water of infinite depth and related free-surface flows. *J. Fluid Mech.*, **240**, 549–557.
23. Wang Z, Milewski PA. 2012. Dynamics of gravity-capillary solitary waves in deep water. *J. Fluid Mech.*, **708**, 480–501.
24. Zakharov VE. 1968. Stability of periodic waves of finite amplitude on the surface of a deep fluid. *J. Appl. Mech. Tech. Phys.*, **2**, 190–194.
25. Zhang X. 1995. Capillary-gravity and capillary waves generated in a wind wave tank: Observations and theory. *J. Fluid Mech.*, **289**, 51–82.